Research Square

Preprints are preliminary reports that have not undergone peer review.
They should not be considered conclusive, used to inform clinical practice,
or referenced by the media as validated information.

Wear Rate Prediction of Multi-Component WC/Co Cermets Using PSO-Optimized Random Forest and XGBoost Models

Riad Harouz

r.harouz@univ-soukahras.dz

Universite Mohamed Cherif Messaadia de Souk-Ahras

Khaled Khelil
Djamel Zelmati
Haithem Boumediri

Research Article

Keywords: WC/Co Cermets, Friction tests, Wear rate, Machine learning (ML), Particle Swarm Optimization

Posted Date: May 6th, 2026

DOI: https://doi.org/10.21203/rs.3.rs-9429192/v1

License: This work is licensed under a Creative Commons Attribution 4.0 International License.
Read Full License

Wear Rate Prediction of Multi-Component WC/Co Cermets Using PSO-Optimized Random Forest and XGBoost Models

Riad Harouz[1*]. Khaled Khelil[2] . Djamel Zelmati[3,4]. Haithem Boumediri[5]

[1]Electromechanical and Operational Safety Laboratory Department of Mechanical Engineering, Faculty of Science and Technology Mohamed Chérif Messaadia University Souk-ahras, Algeria.

[2]Faculty of Science and Technology, LEER Lab, Mohamed Cherif Messaadia University, Souk Ahras 41000, Algeria.

[3]Research Center in Industrial Technologies (CRTI), P.O. Box 64, Cheraga, Algiers, 16014, Algeria.

[4]LRTAPM, Research Laboratory of Advanced Technology in Mechanical Production, Department of Mechanical Engineering, Faculty of Engineering Science, Badji Mokhtar University Annaba, BP 12, 23000, Annaba, Algeria.

[5]Mechanical Department, Institute of Applied Sciences and Techniques, University of Constantine 1, Constantine, Algeria.

*Corresponding,author.
E-mail address: r.harouz@univ-soukahras.dz (Riad Harouz).

Abstract

The accurate prediction of wear rates of WC/Co-based cermets is essential for the development of high-performance industrial components. While machine learning (ML) offers a transformative approach to material design, the lack of specialized, high-fidelity data remains a significant challenge. In this study, an experimental dataset, comprising 116 wear tests WC/Co-based cermets materials with the addition elements, serves as the foundation for this investigation. A robust ML framework is developed to evaluate the performance transition from standard default models to optimized architectures. Specifically, baseline Random Forest (RF) and Xtreme Gradient Boosting (XGBoost) models are compared against variants optimized via the Particle Swarm Optimization (PSO) algorithm. The PSO algorithm was employed for dual-objective optimization, enabling simultaneous feature selection and hyperparameters tuning. Starting from an initial set of 12 input variables, the optimization process reduced the feature space to four predictors for the Random Forest model and nine predictors for the XGBoost model, corresponding to dimensionality reductions of 67% and 25%, respectively. This reduction improves model interpretability while preserving the most informative variables for accurate prediction. Significant performance enhancements were observed when comparing the PSO-optimized variants to the default baseline models. For instance, the PSO-RF model demonstrated an R^2 improvement from 0.8140 to 0.8406, and for the PSO-XGBoost model, the coefficient of determination (R^2) was increased from 0.8234 to 0.8886, representing a 7.92% improvement, while the Root Mean Square Error (RMSE) and Mean Absolute Error (MAE) were reduced by 20.57% and 21.25%, respectively.

Keywords WC/Co Cermets, Friction tests, Wear rate, Machine learning (ML), Particle Swarm Optimization.

1. Introduction

WC/Co-based composite materials (cermets) produced by conventional powder metallurgy techniques are extensively employed in cutting tools, mining equipment, hot forging dies, and other industrial components operating under severe tribological conditions **[1–6]**. To ensure reliable service performance, WC/Co cermets must exhibit excellent wear resistance, dimensional stability, and thermal stability **[7–8]**. The combination of tungsten carbide (WC) as a hard phase and cobalt (Co) as a metallic binder provides an outstanding balance between hardness and toughness, resulting in superior resistance to wear and fracture **[9]**. Owing to their remarkable tribological behavior under high thermo-mechanical stresses, WC/Co-based composites have attracted increasing attention and have undergone significant development in advanced industrial applications **[10]**. Their high thermal stability enables efficient performance at elevated temperatures with limited material degradation, making them indispensable for studying wear mechanisms and extending component lifespan under extreme conditions **[11]**.

Significant improvements in WC/Co-based composites have been achieved through the incorporation of alloying elements such as TiC, Cr, TaC, Ni, and NbC **[12–18]**. These additions aim to optimize tribological operating parameters including normal load, sliding speed, and temperature in order to stabilize the coefficient of friction, minimize wear rate, enhance surface integrity, and prolong service life. Surface degradation in these materials results from complex and interacting wear mechanisms, including abrasive wear, adhesive wear, diffusion, oxidation, and thermal fatigue **[19–24]**.

The literature indicates that experimental variability and material heterogeneity significantly hinder the accurate prediction of tribological performance, particularly with respect to surface hardness **[25–30]**. The wear rate of WC/Co-based composite materials is highly sensitive to tribological parameters such as the coefficient of friction, hardness, and contact surface material, and is strongly dependent on operating conditions, normal load, sliding speed, and temperature, **[31–34]**. These factors make wear rate prediction a high-dimensional, nonlinear problem that can greatly benefit from advanced machine learning (ML) and optimization strategies **[35, 36]**. The tribological performance of WC/Co-based composite materials, particularly in terms of the coefficient of friction and wear rate, is significantly improved by incorporating a percentage of additional elements, resulting in surfaces with enhanced wear resistance, reduced friction, and improved hardness. They enable the production of durable

cermets capable of operating under extreme mechanical and thermal stresses and various operating parameters, particularly in aerospace equipment, hot rolling, and manufacturing tools **[37–40]**.

In tribology, traditional experimental investigations face several challenges, including high costs, time-consuming procedures, and occasional inconsistencies in the obtained results. Comprehensive wear testing typically requires advanced equipment and extended testing durations. Moreover, variations in environmental conditions and material properties can significantly affect the outcomes, thereby limiting reproducibility and reducing the reliability of predictive analyses **[41–44]**.

In this context, ML has emerged as a powerful approach for predicting tribological behavior by integrating experimental observations with numerical datasets **[45–49]**.Traditional experimental investigations are often costly, time-consuming, and occasionally inconsistent due to variations in testing conditions and material properties. ML techniques overcome these limitations by capturing complex nonlinear relationships between material composition, processing parameters, and performance indicators such as friction coefficient and wear rate **[50–52]**. Consequently, ML models enable rapid and reliable predictions, reduce the number of costly experiments, and facilitate efficient material design and optimization.

Among available ML algorithms, ensemble learning methods such as Random Forest (RF) and Extreme Gradient Boosting (XGBoost) have demonstrated strong predictive capabilities in materials science applications **[53–58]**. Their performance can be further enhanced through metaheuristic optimization techniques. Particle Swarm Optimization (PSO), inspired by collective behavior observed in nature, is particularly effective for optimizing model hyperparameters and improving generalization ability **[59–68]**. Therefore, PSO-optimized variants provides a promising strategy for obtaining highly reliable wear rate predictions **[65–68]**.

In the present work, a comprehensive framework was developed to evaluate the effectiveness of PSO for simultaneous feature selection and hyperparameters tuning in wear rate prediction models. Two powerful machine learning algorithms, Random Forest (RF) and eXtreme Gradient Boosting (XGBoost), were employed and their default configurations were systematically compared with PSO-optimized versions. The proposed optimization strategy aims to reduce input dimensionality while improving model performance and interpretability.

The results demonstrate the capability of PSO to efficiently identify the most informative predictors and optimal hyperparameters, leading to more accurate and robust wear rate predictions. The dataset consists of 116 samples with 12 initial features describing material properties and testing conditions. It was randomly divided into training (92 samples, 80%) and testing (34 samples, 20%) sets using a fixed random seed to ensure reproducibility. The PSO optimization aimed to maximize the coefficient of determination (R^2) on the training data through a 5-fold cross-validation strategy, enabling the identification of the most relevant features and the optimal hyperparameters for each algorithm.

2. Materials and methods

This section describes the materials used, the experimental setup, and the procedures adopted for the cermet fabrication process, friction testing, analysis, and wear rate measurements. It also details the modeling techniques applied to predict friction test performance and optimize tribological parameters.

2.1 Experimental setup

2.1.1 Materials preparation

The materials cermets preparation procedure from mixtures manufactured in the laboratory by mixing powders of medium grain size **Fig. 1.** The materials (cermets) of shades based on tungsten carbide (WC), cobalt (Co) binder and addition elements of TiC, Ni, Cr, TaC, and NbC, which form eight shades. **Table 1** illustrates the content range of all constituents within all cermets.

Table 1 Range of contents of the basic composition and the addition elements of the elaborated cermets

Addition elements of cermet	WC	Co	TiC	Cr	Ni	TaC	NbC
Range of contents	70%−85%	10%−15%	0%−15%	0%−5%	0%−10%	0%−5%	0%−5%

Eight grades were fabricated with different compositions, each having a cylindrical geometry of 35 mm in diameter and 15 mm in thickness **Table 2**.

Table 2 The composition of different grades

Grades / Elements addition	WC	Co	TiC	Cr	Ni	TaC	NbC
G1	85%	15%	0%	0%	0%	0%	0%
G2	80%	15%	5%	0%	0%	0%	0%
G3	75%	15%	10%	0%	0%	0%	0%
G4	70%	15%	15%	0%	0%	0%	0%
G5	75%	15%	5%	5%	0%	0%	0%
G6	75%	10%	10%	0%	5%	0%	0%
G7	70%	10%	5%	0%	10%	5%	0%
G8	70%	10%	5%	0%	10%	0%	5%

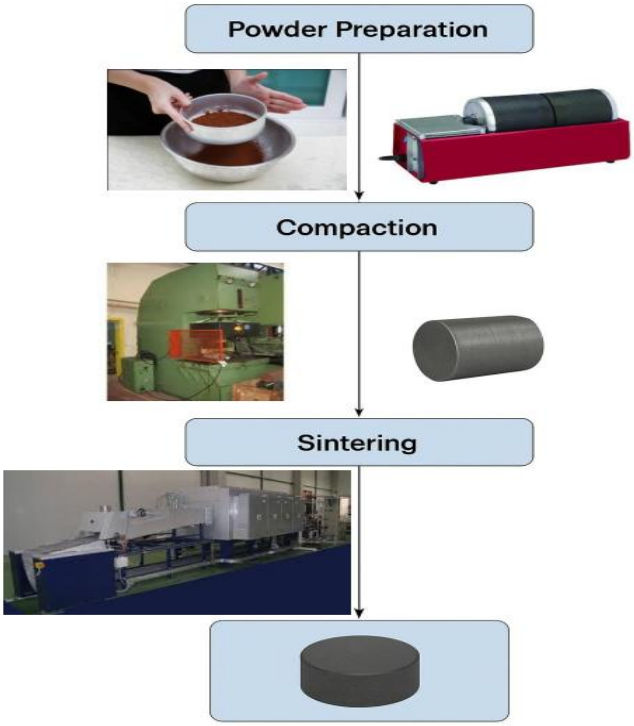


Fig.1. Cermet preparation procedure

The mean hardness and the density tests of different grades, carried out using INDUNO OLONA-VA-ITALY device and Archimedes method respectively, have shown that the obtained samples comply with ISO standards as reported in **Table 3.**

Table 3 Density and hardness mean values of the height elaborated WC/Co-based cermets

Grade	G1	G2	G3	G4	G5	G6	G7	G8
Mean density (g/cm^3)	71.60	74.40	77.70	77.70	57.60	68.00	66.40	68.20
Mean hardness (HRC)	13.84	11.74	10.70	10.70	10.71	12.74	11.50	11.97

2.1.2 Friction tests method

The tribological behavior of the samples was evaluated through high-temperature friction and rotary sliding tests using a tribometer (CSM Instruments, Switzerland), as shown in **Fig. 2**. Eight cermet grades were investigated using an alumina (Al_2O_3) ball with a diameter of 6 mm, hardness of 1800 HV, and density of 3.2 g/cm^3. A total of 116 friction tests were performed at four different radius under various experimental conditions, including normal load, temperature, sliding speed, and sliding distance (**Table 4**).

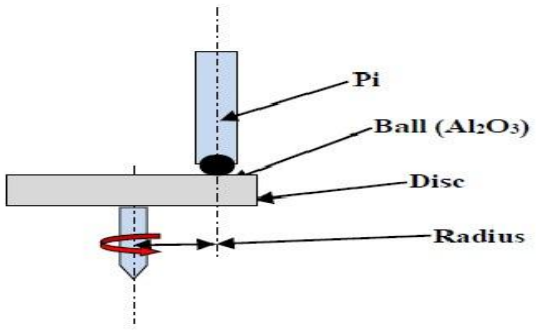


Fig. 2 Friction test process between the Al_2O_3 ball and disc (cermets)

Table 4 Parameters of friction tests

	Parameters of friction tests			
Levels of parameters	Applied load P (N)	Sliding speed V (m/s)	Contact temperature T (°C)	Traveled distance D (m)
Level 1	20	0.5	20	5000
Level 2	20	0.5	450	5000
Level 3	20	0.75	450	5000
Level 4	20	0.5	650	5000

The ball rubs against the surfaces of the test samples in such a way that the wear track is a circle of radius (5mm), centered on the test cermet (disc) **Fig. 2.** The friction force, the friction coefficient, the humidity, the track temperature and the furnace temperature are regularly recorded throughout with the acquisition time in seconds using the software (Tribometer module/Version 4.4.Q).

The grades were tested under dry sliding conditions against an Al_2O_3 ceramic counterface to evaluate the coefficient of friction (μ), which exhibited average values ranging from 0.4 to 0.65.

2.1.3 Wear rate measurement steps

The wear rate measurement procedure is illustrated in **Fig. 3**. Surface profiles were acquired along the worn track using a surface profilometer coupled with a three-dimensional (3D) optical microscope (Contour GT-I, Bruker Nano Surfaces Division, Tucson, AZ, USA), as presented in **Fig. 3(a)**. The analysis procedure consists in using software (vision) to analyse the wear track image as illustrated in **Fig. 3(b)**. This analysis gives a geometrical relief of the wear track (profile of the worn track) of the test sample **Fig. 3(c).** The wear track volume is characterised by the depth (in μm) measured with respect to the surface of the sample, the width (in mm) and the perimeter (in mm) of the wear track given by an optical profiler. Four equally spaced measurements were taken on each circle track (90° between two successive points), **Fig.4**.

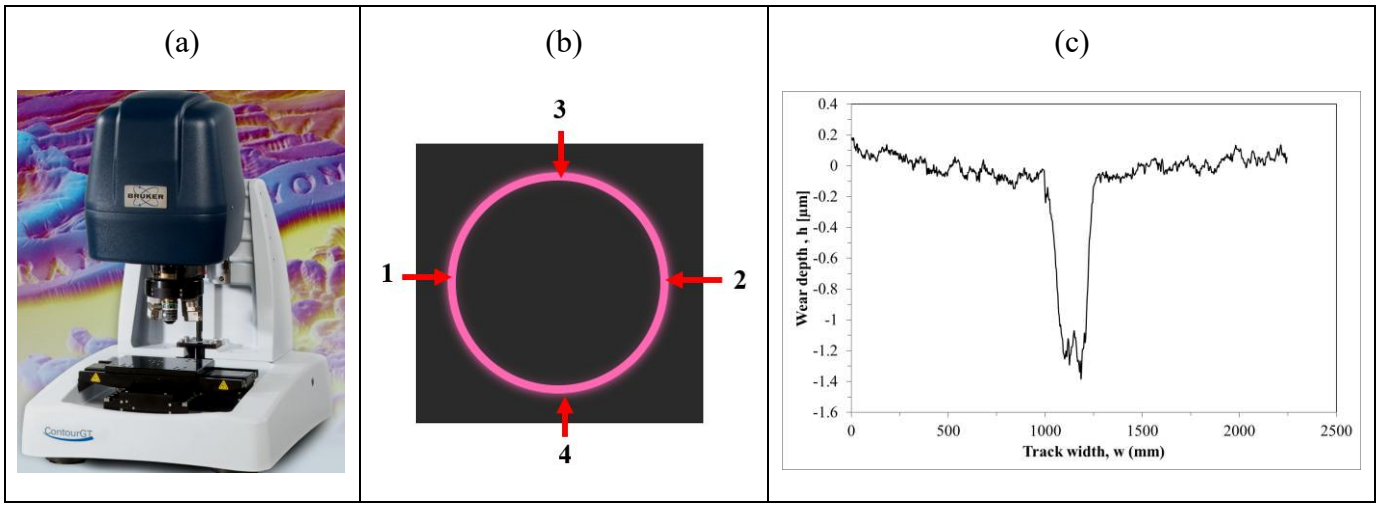


Fig. 3 Wear rate measurement procedure (a) Surface profilometer the three-dimensional (3D) optical microscope (b) Trace of the wear track after a friction test (c) Wear track width (mm) and depth profile (μm)

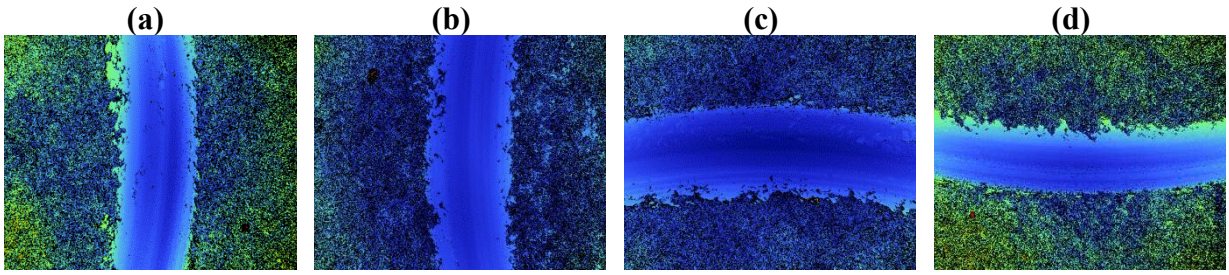


Fig.4 The four sections measured by the optical profile meter of each track, spaced 90° apart, to measure the average worn volume

The worn surface area was measured and multiplied by the perimeter of the wear track to obtain the worn volume V. The wear rate (K) was then calculated from the worn volume V (μm^3) for a sliding distance of D = 5000 m under a normal load of P = 20 N.

$$K = \frac{V}{P.D} \qquad (\mu m^3/N/m) \tag{1}$$

3. Machine learning methodology

3.1 Flowchart wear rate prediction

The flowchart presented in **Figure 5** describes an organized and comprehensive research structure for the development and measurement of wear rate, using XGBOOST and RF machine learning and the PSO optimization method. This structure utilizes composite materials and methods, process parameter selection, experimental design, machine learning, and evolutionary optimization to improve process understanding and the tribological performance of cermet production.

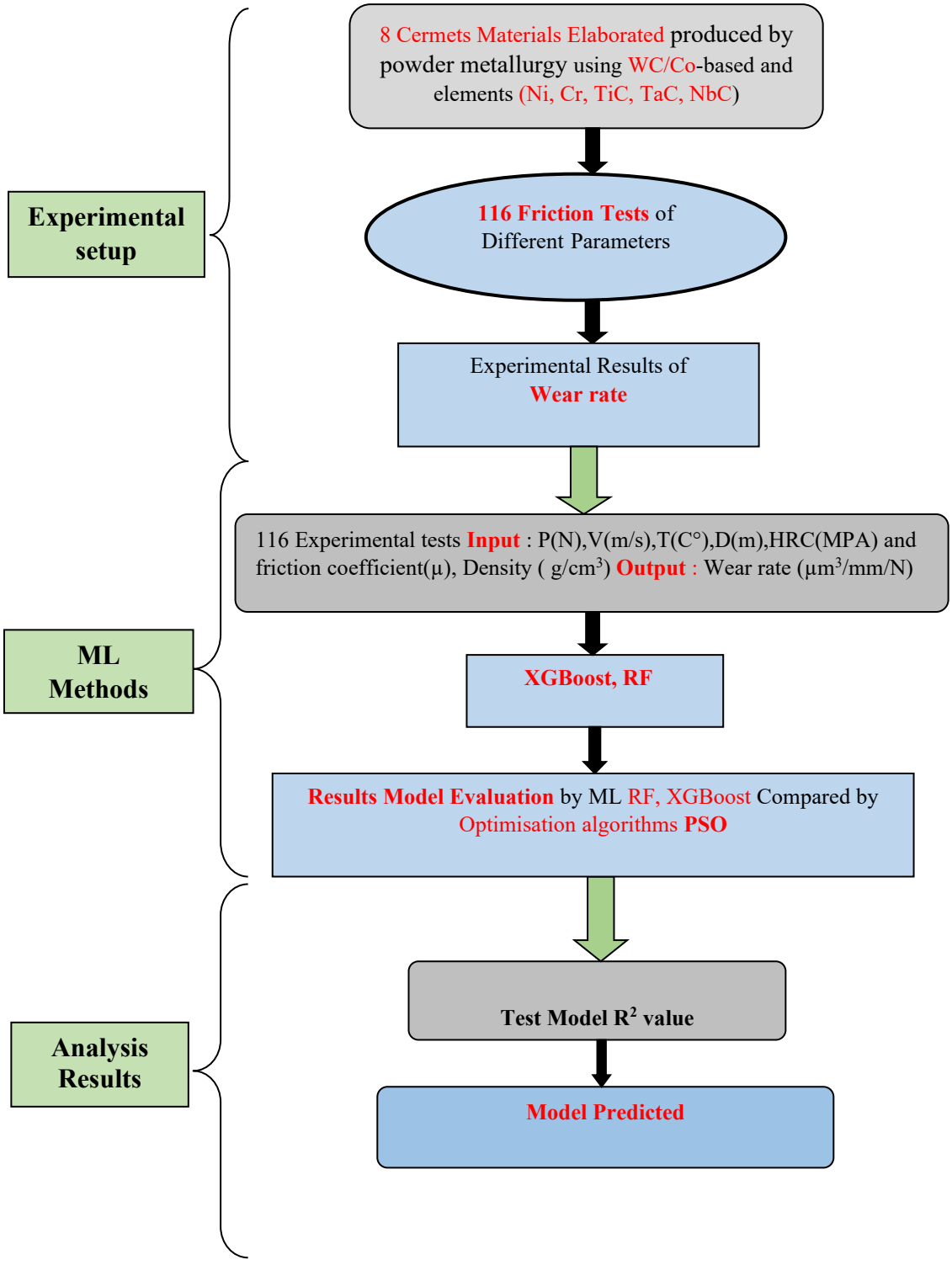


Fig. 5 Flowchart wear rate prediction of the optimization process by experimental setup and ML Method

3.2 Data set input factors and target

The experimentally measured wear volumes and the corresponding wear rates for each combination of input parameters, as presented in **Table 5**, reveal distinct trends.

Table 5. Summary of mean input and output variables for the eight WC/Co-based cermets investigated in this study.

	Input parameters					Target
Cermet	T (°C)	V (m/s)	Hardness (HRC)	Density (g/cm^3)	μ (mean)	Wear rate (μm^3/mm/N)
G1	450	0.75	69	13.86	0.4	178.85
G2	450	0.75	71.6	13.84	0.91	181.19
G3	450	0.75	74.4	11.74	0.63	189.69
G4	450	0.75	77.7	10.7	0.54	268.47
G5	450	0.75	57.6	10.71	0.56	269.78
G6	450	0.75	68	12.74	0.48	301.99
G7	450	0.75	66.4	11.5	0.52	476.67
G8	450	0.75	68.2	11.97	0.44	554.69

3.3 Baseline models

3.3.1 Random forest

Our goal, then, is to choose a set of hyperparameters that navigates this trade of between bias and variance so as to minimize error (or maximize goodness-of-ft) on some new set of data (the validation set) that we believe is representative of what the model might encounter when solving the real world problem it was designed for (the test set).

RF regression is an ensemble model machine learning-based method that improves predictive probability by combining models. Using bagging, a number of learner trees are created which are then ensembled to work together as an ensemble and obtain the overall prediction. Each tree independently makes a prediction or classification, and the final output of the Random Forest model is determined by the prediction or classifcation that receives the majority vote. The idea behind Random Forest is that a group of independent decision trees, acting as a committee, performs better than any single decision tree alone. Although a RF model has limited interpretability and relatively high training complexity, it achieves a good balance between bias and variance, delivers high accuracy, and minimizes overfitting by incorporating regularization techniques like dropout and early stopping **[53–58]**. It can be expressed by **Eq. (2)**:

$$\widehat{m}(x) = \frac{1}{M} \sum_J \widehat{m_j}(x) \quad \textbf{(2)}$$

3.3.2 XGBoost

Extreme gradient boosting XGBoost, one of the most efficient ensemble machine learn-ing techniques belonging to the family of GB algorithms, was frst introduced by Chen and

Guestrin **[53–58]**. XGBoost is also an implementation of gradient-boosted decision trees and a powerful tool for highly parallelized boosting of trees. For XGBoost, the cost function C is composed of a loss function and a regularization term, as expressed by **Eq. (3):**

$$C(\theta) = L(\theta) + \Omega\,(\theta) \tag{3}$$

Here, Θ represents the model parameters, L denotes the loss function, and Ω is the regularization term. The loss function is typically chosen as the mean squared error (MSE). The regularization term helps prevent overfitting by controlling model complexity and balancing bias and variance to ensure the model remains both simple and predictive. Although less interpretable than simpler models, XGBoost ofers insights into feature importance, highlighting the factors that most influence predictions. Additionally, XGBoost effectively manages the bias-variance trade of and generalizes well to unseen data, though it may require complex hyperparameters tuning **[53–58]**.

4. PSO-Based Model Optimization

The predictive modeling of wear rates in cemented carbides requires a nuanced understanding of the intersection between metallurgical composition, environmental stressors, and algorithmic logic. This investigation successfully implemented a Particle Swarm Optimization (PSO) framework to refine two prominent ensemble learners: Random Forest (RF) and Extreme Gradient Boosting (XGBoost). By utilizing a hybrid wrapper approach for feature selection and simultaneous hyperparameters tuning, the obtained results indicate that the method yields high predictive accuracy while effectively minimizing the feature space.

4.1 Particle Swarm Optimization overview

Particle Swarm Optimization (PSO) algorithm, introduced in 1995 by Kennedy and Eberhart, is a stochastic search technique inspired from the collective intelligent behavior of animal societies such as ant colonies, bird flocks, or fish schools. PSO aims at finding the optimal solution for a given multidimensional problem, where each candidate solution, called a particle, representing a point in the *N*- dimensional search space, where N is number of variables of the function to be optimized. PSO performs search starting from a random swarm of particles, called initial population, that emulate the success of neighboring members to achieve their own successes. Alternatively, using shared information amongst the swarm of individuals, each particle updates its velocity and position based on its current and past trajectories.

Originally proposed by Kennedy and Eberhart in 1995 **[67–69]**, Particle Swarm Optimization (PSO) is a stochastic, population-based metaheuristic inspired by the synchronized social behavior of animal collectives, such as bird flocks or fish schools. Unlike evolutionary strategies that rely on "survival of the fittest," PSO is built on the principle of cooperative intelligence.

Consider the optimization problem involving *N* variables (corresponding to the number of features). For a population of size *P*, each particle $p_i(i = 1,2, \dots, P)$ at iteration *t* is characterized by a position $p_i(t) \in \mathcal{R}^N$, velocity $v_i(t) \in \mathcal{R}^N$, and personnel best position $P_{bi}(t) \in \mathcal{R}^N$ representing the optimal solution discovered by the particle during its search history.

Let $P_g(t) \in \mathcal{R}^N$ denote the global best position discovered across the entire swarm up to iteration *t*. The dynamics governing the motion of each particle during the optimization process are described by the following update equations **[69,70]**:

$$\begin{cases} v_i(t+1) = \omega\, v_i(t) + c_1.r_1[P_{bi}(t) - p_i(t)] + c_2.r_2\left[P_g(t) - p_i(t)\right] \\ p_i(t+1) = p_i(t) + v_i(t) \end{cases} \quad \textbf{(4)}$$

Where, ω represents the inertia weight, which balances local exploitation and global exploration, higher values of facilitate ω broader exploration of the search space. The acceleration coefficients c_1, c_2 correspond to the cognitive and social components, respectively, controlling the influence of the particle personal best and the swarm global best on its velocity update. r_1 and r_2 are random variables taking values from a uniform distribution in the interval [0,1].

4.2 Feature selection and Hyperparameters optimization

The optimization process utilized a Particle Swarm Optimization (PSO) algorithm designed to navigate a complex, multi-dimensional search space consisting of both discrete (feature selection) and continuous (hyperparameters) variables.

4.2.1 The fitness function

The optimization process relies on a fitness (cost) function to evaluate the solutions encoded by particle positions. This work utilizes a weighted multi-objective function that prioritizes predictive accuracy R^2 and includes a penalty term for model complexity, based on the number of selected features. The cost *J* is expressed as:

$$J = \alpha(1 - R^2) + (1 - \alpha)\left(\frac{N_{selected}}{N_{total}}\right) \quad \textbf{(5)}$$

where α is a weighting factor set to 0.95 to prioritize model accuracy over feature parsimony. The term $N_{selected}$ represents the number of features selected in a given subset, and N_{total} denotes the total number of available features. This formulation ensures that the swarm converges on a solution that explains the maximum variance with the minimum number of descriptors.

4.2.2 Algorithm steps and execution:

The PSO algorithm followed a structured iterative process to evolve the swarm toward the global best solution P_g :

1) **Initialization:** A swarm of N particles is generated. Each particle position vector includes a binary mask for feature selection and continuous values for the model hyperparameters (e.g., $n_estimators$, max $_depth$, etc.).
2) **Binary Mapping:** For feature selection, continuous position values are mapped to a binary representation (1 or 0) based on a threshold of 0.5. A value of 1 indicates that the corresponding feature is included in the current model iteration, while a value of 0 signifies its exclusion.
3) **Model Training and Evaluation:** For each particle, a model is trained using the selected features and hyperparameters. The performance is measured on a test set using R^2, $RMSE$, and MAE.
4) **Fitness Calculation:** The cost is calculated using the fitness function described by equation **(5)**
5) **Personal best and global best update:**
   - The personal best position P_b is updated whenever a particle attains a cost value lower than its previous best.
   - The global best P_g is replaced when a particle discovers a position yielding a cost value lower than the current swarm optimum.
6) **Velocity and Position Update:** Particle velocities and positions are updated using equations **(4).**

Termination: Steps 2–6 are executed iteratively until either the maximum number of iterations is reached or the global best cost P_g stabilizes, indicating convergence.

4.3 Evaluation of ML model Performance

Performance metrics offer quantitative assessments of the alignment between machine learning models and experimental data. The coefficient of determination R^2 is indeed a widely used metric for evaluating the performance of ML models in regression tasks. A value of R^2 in the range of 70% to 90% shows that the model is doing well, meaning its predictions closely match the actual data. In addition, mean absolute error (MAE), mean squared error (MSE), and root mean squared error (RMSE) were used to evaluate model performance **[71]**. Thus indicating the wear rate's experimental value as Wj and the predicted value as Xj, where j = 1, 2, ⋯, n is the sample size, and the four metrics measurements are specified below:

Determination coefficient (R^2)

$$R^2 = 1 - \frac{\sum_{j=1}^{n}(Xj - Wj)^2}{\sum_{j=1}^{n}(Xj - \overline{W})^2} \quad , \tag{6}$$

Root mean squared error (RMSE)

$$RMSE = \sqrt{\frac{\sum_{j=1}^{n}(Xj - Wj)^2}{n}}, \tag{7}$$

Mean absolute error (MAE)

$$MAE = \frac{\sum_{j=1}^{n}(Xj - Wj)}{m} \quad , \tag{8}$$

Relative absolute error (RAE) and where $\overline{w}$ is the mean sample in the dataset.

$$RAE = \frac{\sum_{j=1}^{n}(Xj - Wj)}{\sum_{j=1}^{n}(Xj - \overline{W})} \quad . \tag{9}$$

5. Results and Discussion

5.1 Proposed Setup and Methodology

The experimental framework was designed to evaluate the effectiveness of Particle Swarm Optimization (PSO) for simultaneous feature selection and hyperparameters tuning in wear rate prediction models. The study employed two powerful machine learning algorithms, Random Forest (RF) and eXtreme Gradient Boosting (XGBoost), comparing their default configurations against PSO-optimized versions. The dataset comprised 116 samples with 12 initial features describing material properties and testing conditions. This was randomly split into training (92 samples, 80%) and testing (24 samples, 20%) sets using a fixed random seed for reproducibility. The PSO process aimed to maximize the model coefficient of determination (R^2 score) on the training data through a 5-fold cross-validation strategy,

thereby identifying the most relevant features and optimal hyperparameters for each algorithm while guarding against overfitting.

5.2 Performance Comparison of PSO-Optimized Models against Default Models

The PSO optimization process yielded significant performance improvements for both models, with the gains validated on the unseen test set. The results, summarized in **Table 6**, underscore the power of this hybrid approach.

5.2.1 Random Forest performance analysis

The PSO-optimized Random Forest model demonstrated a robust improvement over its default counterpart. It achieved an R^2 score of 0.84, a 2.66% increase from the default model 0.81. More importantly, the model prediction errors were substantially reduced. The RMSE decreased by 7.43% from 99.91 to 92.49 $\mu m^3/m/N$, and the MAE saw a notable improvement of 10.84%, dropping from 78.00 to 69.54 $\mu m^3/m/N$. **Table 6** illustrates the performance comparison of PSO-Optimized and Random Forest Default Models

A key achievement of the PSO optimization was the dramatic simplification of the model. It identified an optimal feature subset of only 4 out of the 12 original features: TaC (Tantalum Carbide), T (Temperature), D (Density), and μ (Mean friction coefficient) . This represents a 67% reduction in input dimensionality. This simplification not only enhances model interpretability but also significantly reduces the computational burden and data collection requirements for future predictions, all while improving predictive accuracy. The selection of TaC and T aligns with domain knowledge, highlighting the critical influence of hard carbide phases and thermal conditions on wear. The inclusion of Density and the mean friction coefficient suggests that the material compactness and the frictional behavior at the contact interface are also primary drivers of wear.

Table 6 Performance Comparison of PSO-Optimized and Random Forest Default Models

Model	PSO- RandomForest	Default-RandomForest	Improvement
R^2	0.81	0.84	+2.66%
RMSE ($\mu m^3/m/N$)	99.91	92.49	-7.43%
MAE ($\mu m^3/m/N$)	78	69.54	-10.84%
No. of Features	4	12	-67%

5.2.2 XGBoost performance Analysis

The PSO-optimized XGBoost model achieved even more substantial performance gains. Its R^2 score soared to 0.89, a remarkable 6.52% improvement over the default model 0.82. The reduction in error metrics was also more pronounced than for Random Forest. The RMSE was slashed by an impressive 20.57%, from 97.36 to 77.33 ($\mu m^3/m/N$), and the MAE was reduced by 21.26%, from 74.14 to 58.38 ($\mu m^3/m/N$). These substantial reductions in error metrics, exceeding 20%, indicate that the PSO-optimized XGBoost model is exceptionally precise and its predictions are, on average, much closer to the true values. **Table 7** illustrates Performance Comparison of PSO-Optimized and XGBoost default models. For XGBoost, PSO identified a larger optimal feature subset of 9 features, including Co, TiC, Ni, TaC, NbC, T, V, HRC, and μ (Mean Friction Coefficient). This selection provides a more comprehensive view of the factors influencing wear, incorporating binder elements (Co, Ni), various carbides (TaC, NbC, TiC), mechanical properties (HRC), and interfacial mean friction coefficient (μ). While the feature reduction is only 25%, the primary benefit here is the dramatic performance gain achieved through both feature selection and, crucially, hyperparameters tuning.

Table 7 Performance Comparison of PSO-Optimized and XGBoost Default Models

Model	PSO-XGBoost	Default-XGBoost	Improvement
R^2	0.82	0.89	+6.52%
RMSE ($\mu m^3/m/N$)	97.36	77.33	-20.57%
MAE ($\mu m^3/m/N$)	74.14	58.38	-21.26%
No. of Features	0.82	0.89	-25%

Based on the obtained results, the superior performance of the PSO-optimized models, particularly XGBoost, is further highlighted by their more consistent and balanced error distributions. The optimized XGBoost model, exhibiting substantially lower error metrics (RMSE reduced by 20.57% and MAE reduced by 21.26%), shows a much narrower error distribution clustered around zero compared to its default counterpart. This indicates a model that is not only more accurate on average but also more reliable, with fewer large-magnitude prediction errors. The substantial improvement in XGBoost error metrics, over twice that seen for Random Forest, indicates that the default XGBoost model was particularly susceptible to

overfitting or suboptimal hyperparameters settings, which the PSO optimization effectively addressed.

Fig. 6 provides a comparative analysis of the R^2, RMSE and MAE metrics for the baseline models and their PSO-optimized versions. The findings indicate that the incorporation of PSO substantially improves the predictive performance of both the Random Forest and XGBoost algorithms relative to their default parameter settings. For instance, both PSO-optimized models exhibit superior performance relative to their default configurations, confirming the effectiveness of the integrated feature selection and hyperparameters tuning strategy. For the Random Forest model, PSO optimization refines key structural parameters (e.g., number of trees, maximum depth, and feature sampling), thereby reducing estimator variance and improving ensemble stability. This leads to a more consistent aggregation of decision trees and mitigates overfitting caused by suboptimal parameter settings. Besides, in the case of XGBoost, PSO tuning adjusts critical boosting parameters (e.g., learning rate, maximum depth, regularization coefficients, and number of boosting rounds), enhancing the gradient-based optimization process. By better controlling shrinkage and regularization, the optimized model achieves improved convergence behavior and a more favorable bias–variance balance.

Quantitatively, for the Random Forest model, PSO-based optimization reduced the RMSE and the MAE This reduction indicates a meaningful contraction of the prediction error distribution, reflecting improved predictive accuracy. The optimization refines critical ensemble parameters such as the number of trees, maximum depth, and feature sampling strategy, which reduces estimator variance and mitigates overfitting while maintaining model flexibility.

For the XGBoost model, the improvements are even more pronounced. The RMSE and MAE decrease indicate a substantial reduction in prediction errors and enhanced generalization capability. PSO tuning adjusts key boosting parameters, including learning rate, maximum depth, regularization coefficients, and number of boosting rounds. By controlling shrinkage and regularization more effectively, the optimized model achieves better bias–variance balance, improved convergence, and reduced overfitting risk.

PSO-optimized models across both Random Forest (RF) and XGBoost algorithms, the R^2 values demonstrates a substantial improvement achieved through PSO-based joint optimization of feature selection and hyperparameters. Notably, the PSO-XGBoost model determination coiefficient of 0.89, indicates a strong predictive accuracy on the test set. These

gains correspond to a substantial reduction in prediction errors, as reflected in the RMSE and MAE values shown in **Fig. 6**, and demonstrate that the optimized model produces predictions that are significantly closer to the experimental values. In addition, PSO-optimized models reduced the feature set by 60% for both models, simplifying the models, mitigating overfitting, and improving interpretability, while maintaining or enhancing predictive accuracy. **Fig. 7** illustrates the performance metrics improvement and feature reduction percentages for the proposed PSO-optimized models compared to standard default configurations.

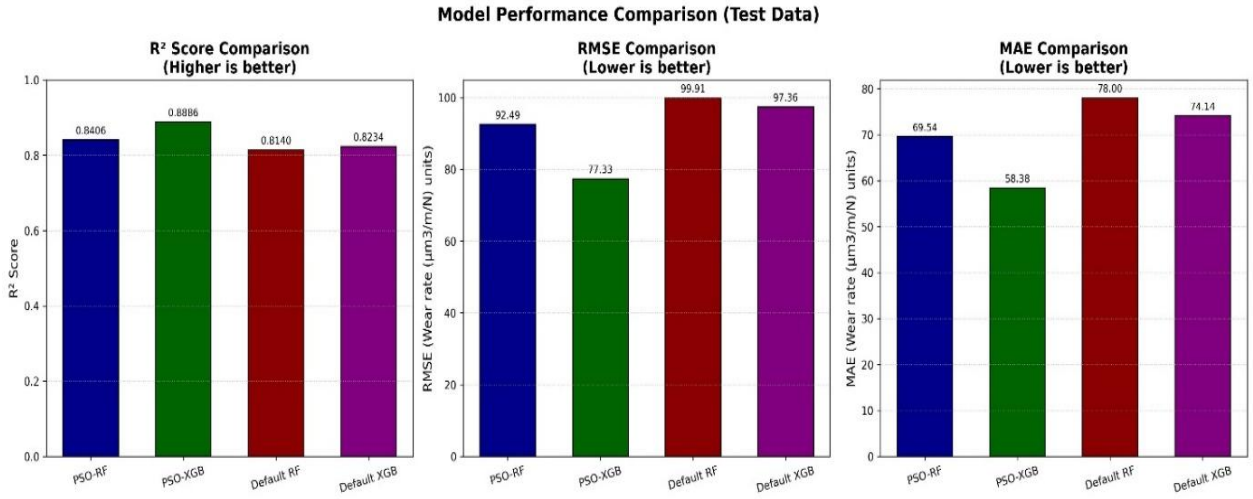


Fig. 6. Comparison of R^2 scores demonstrating improved predictive accuracy with PSO optimization.

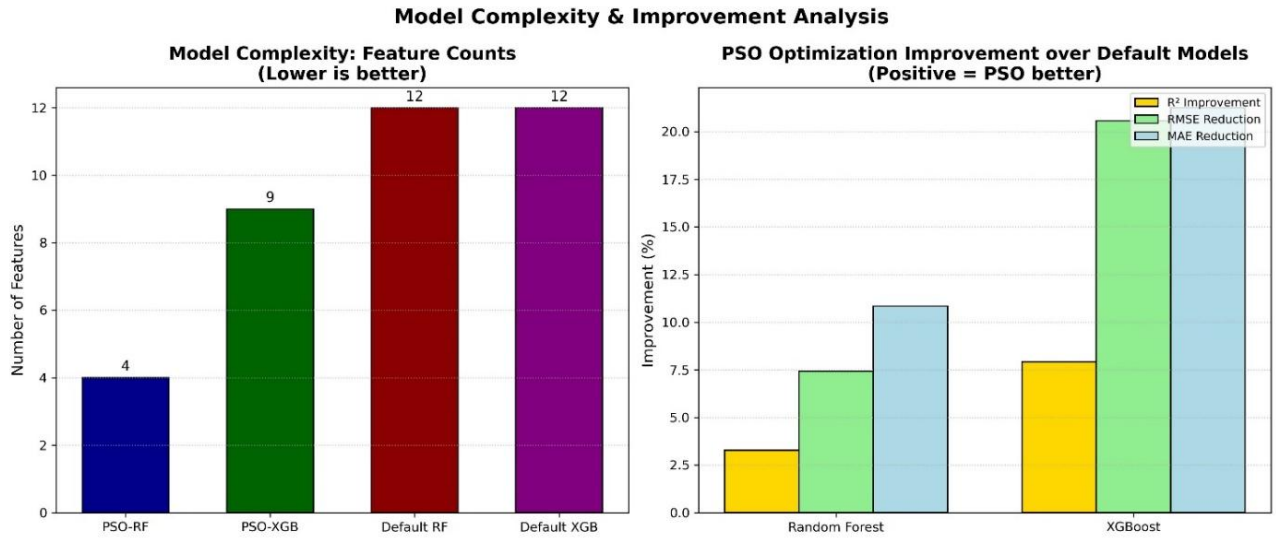


Fig. 7 Performance metrics improvement and feature reduction percentages for the proposed PSO-optimized models compared to standard default configurations

It is obvious that the proposed PSO-optimized models show a closer agreement with the experimental data compared to the default configurations. **Fig. 8** and **Fig. 9** illustrate the comparison between measured (experimental) and predicted wear rates for the PSO-optimized models and the corresponding standard baseline models. This improved alignment demonstrates that PSO-driven feature selection and hyperparameters tuning enhance predictive accuracy, reduce error variance, and improve model generalization,highlighting that both ensemble algorithms benefit from PSO optimization, with XGBoost showing the most pronounced reduction in prediction error. For the Random Forest model results, the predictions generated by the PSO-optimized version cluster more tightly around the 45° line compared to those from the standard model. This tighter clustering reflects reduced residual variance and enhanced predictive consistency. In contrast, the baseline Random Forest model exhibits greater scatter and more pronounced deviations from the ideal line, indicating higher prediction errors and less stable generalization performance.

The PSO-based hybrid optimization effectively identified highly informative feature subsets and tuned hyperparameters for both Random Forest (RF) and XGBoost models, improving prediction accuracy and model robustness. Notably, Random Forest achieved optimal performance with only 4 features, while XGBoost required 9 features to capture more complex relationships in the data, highlighting the different sensitivities and learning capacities of the two algorithms. **Table 8** and **Table 9** Summarize the best Feature Subset and Hyperparameters for the both PSO-Optimized Random Forest and XGBoost Models.

These results demonstrate that PSO optimization successfully balances feature reduction and parameter tuning. For Random Forest, the moderate tree depth and high min_impurity_decrease ensure reliable predictions using only 4 features. In contrast, XGBoost requires more trees with lower depth, moderate learning rate, and subsampling strategies to efficiently leverage 9 features while controlling overfitting. Overall, the PSO process adapts to the specific requirements of each algorithm, resulting in models that are both accurate and robust, with improved interpretability and reduced risk of large-magnitude prediction errors.

Table 8. Best Feature Subset and Hyperparameters for the PSO-Optimized Random Forest Model

Category	Parameter / Feature	Value
Feature Subset	Count	4/12
	Features	TaC, Temperature, Density, μ
Hyperparameters	n_estimators	387
	max_depth	6
	Min_samples_split	2
	Min_samples_leaf	1
	Max_features	1
	Min_impurity_decrease	0.1912
	ccp_alpha	0.05

Table 9. Best Feature Subset and Hyperparameters for the PSO-Optimized XGBoost Model

Category	Parameter / Feature	Value
Feature Subset	Count	9/12
	Features	Co, TiC, Ni, TaC, NbC, Temperature, V, Hardness, μ
Hyperparameters	n_estimators	846
	Max_depth	3
	Learning_rate	0.2904
	Subsample	0.6148
	Colsample_bytree	0.6835
	Gamma	0.0129
	reg_alpha	0.8095

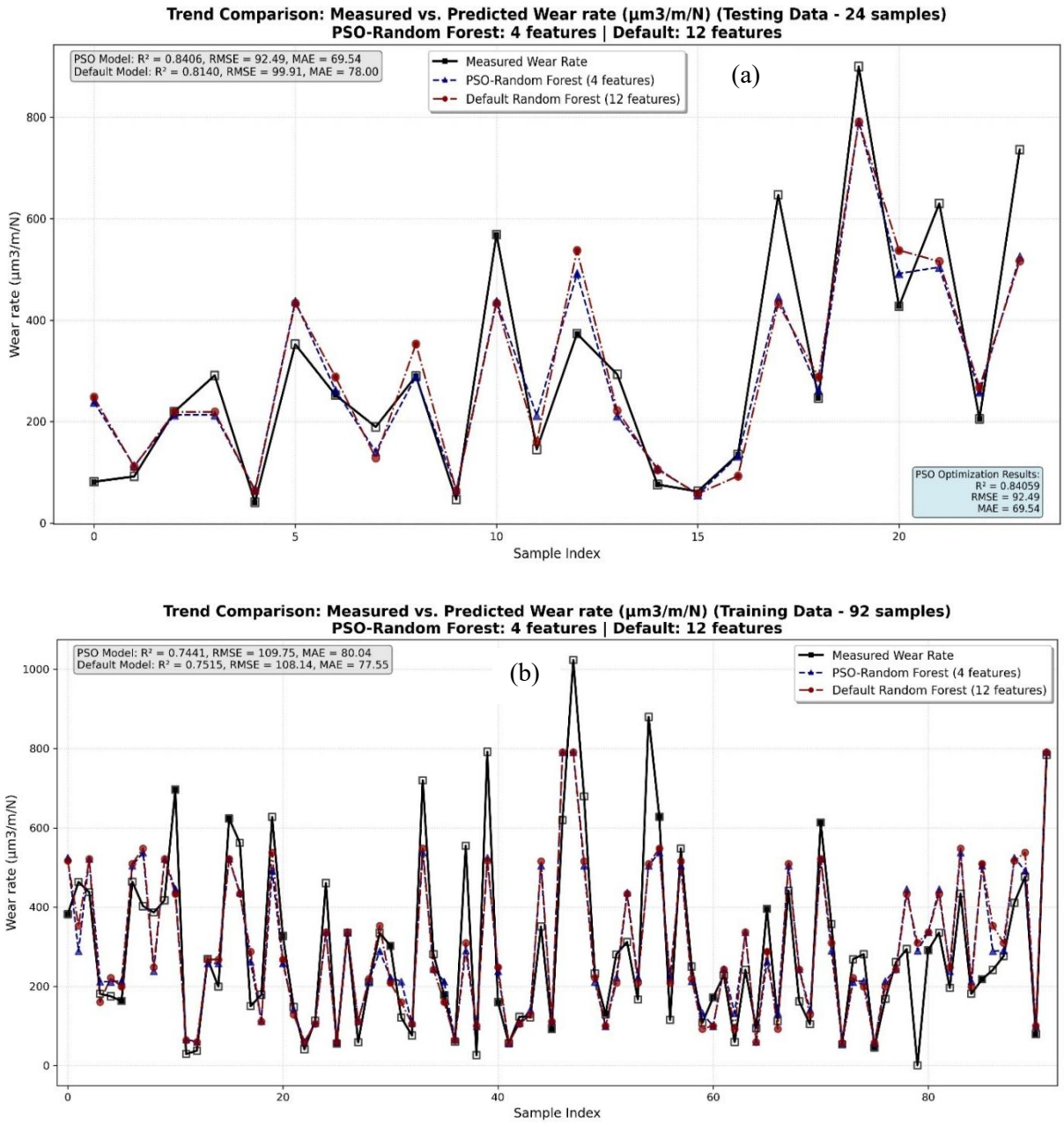


Fig. 8 Experimental and predicted wear rates using the standard and PSO-optimized Random Forest model: (a) testing set, (b) training set.

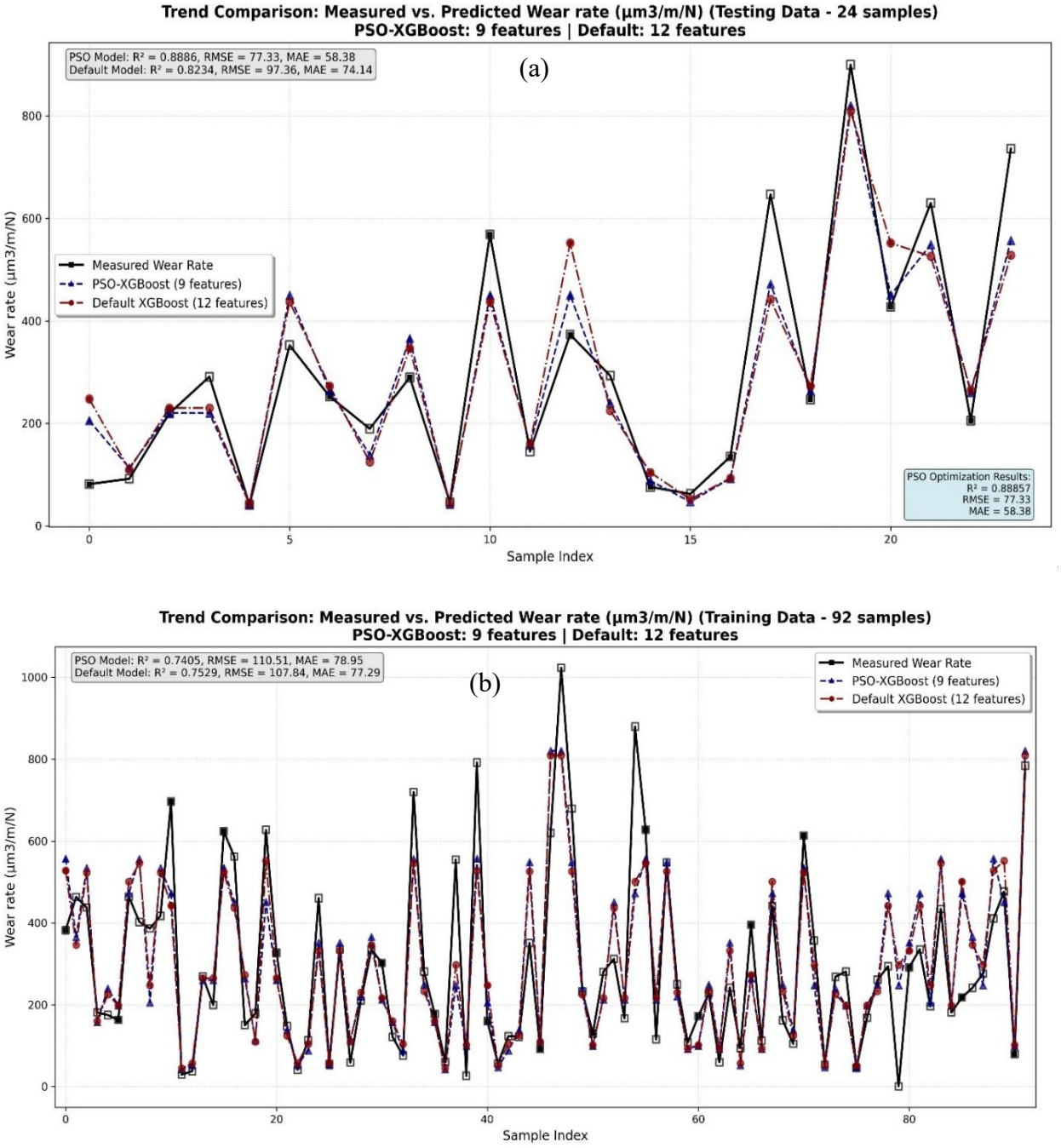
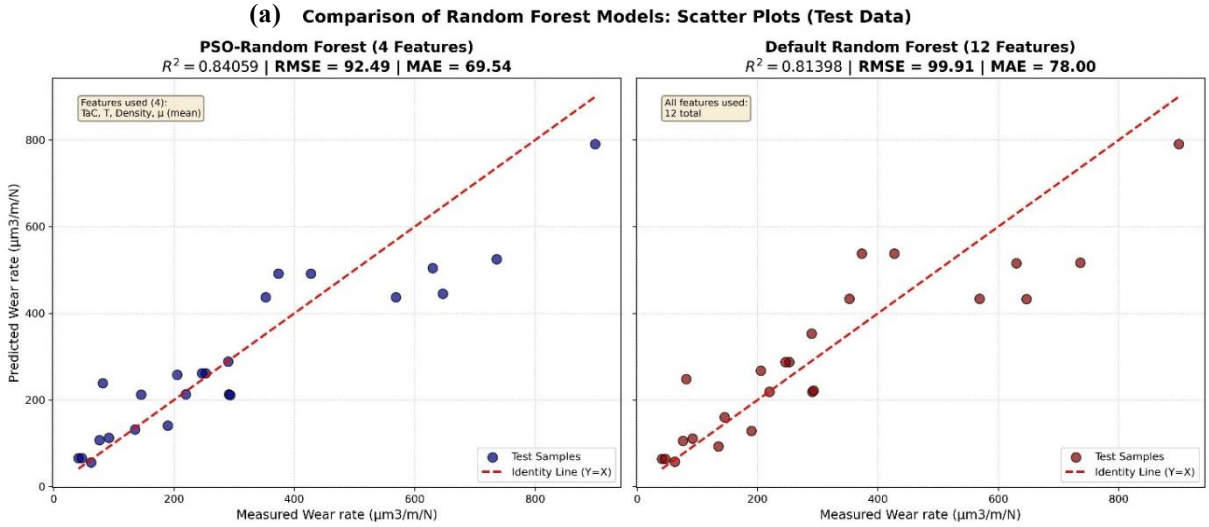


Fig. 9 Experimental and predicted wear rates using the standard and PSO-optimized XGBoost model: (a) testing set, (b) training set.

In fact, it is very interesting to know that for both algorithms, the PSO-optimized models exhibit a tighter clustering of data points around the 45° reference line, indicating improved agreement between predicted and experimental values. Despite the substantial reduction in input dimensionality (67% and 25% feature reduction for Random Forest and XGBoost respectively), the optimized models not only maintain predictive performance but enhance it, as evidenced by reduced dispersion and lower residual magnitude. Besides, **Figure 10**

illustrates the feature importance rankings for both the standard and PSO-optimized models, providing insight into how the optimization process identified a compact yet highly predictive subset of input variables. The baseline models, trained on all 12 initial features, distribute importance across multiple predictors, including several variables with only marginal contributions to the predictive function. In contrast, for the Random Forest algorithm, the PSO-optimized model retains only four features (T, TaC, WC, and Cr), corresponding to a 67% reduction in dimensionality. This substantial reduction suggests that Random Forest can achieve strong predictive performance using a compact subset of highly informative variables, likely due to its ensemble averaging mechanism, which reduces variance even with fewer predictors.

For the XGBoost algorithm, the PSO-optimized model retains six features (TaC, T, NbC, HRC, TiC, and Cr), corresponding to a 25% reduction in dimensionality. The retention of a slightly larger feature subset may reflect the gradient boosting framework's sequential learning mechanism, which can benefit from additional complementary predictors to iteratively minimize residual errors.



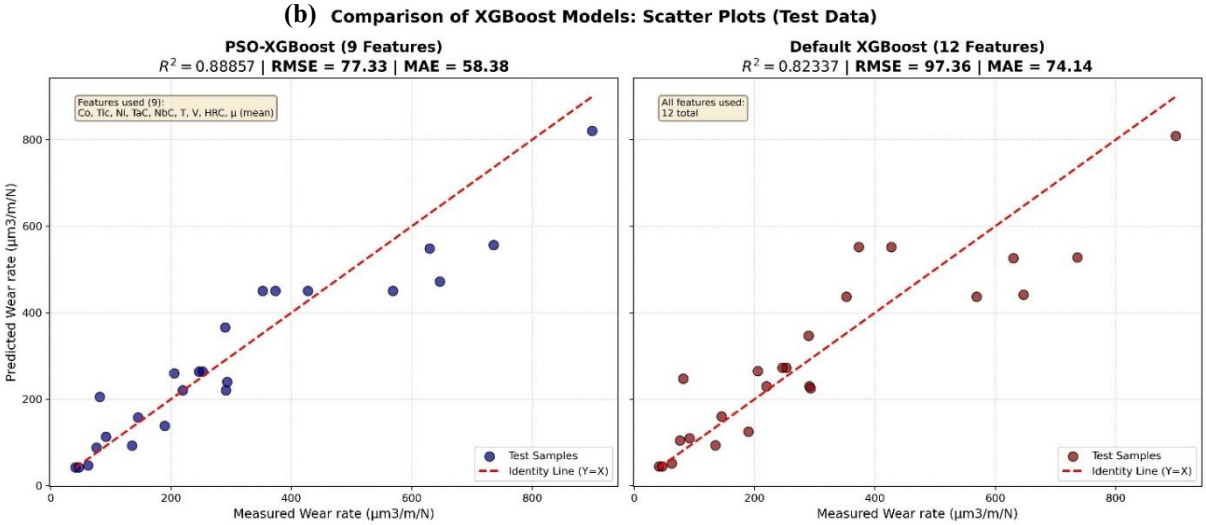


Fig.10 Measured versus Predicted Wear Rate with ideal 45° agreement line (a) Random Forest model and (b) XGBoost Model

These retained variables consistently rank among the most influential predictors in the baseline models, confirming that the PSO algorithm effectively maximizes predictive relevance while minimizing redundancy. This reduced model improves interpretability and leads to lower prediction errors (RMSE and MAE), as shown in **Fig. 9 and Fig. 10**. The feature importance plots therefore provide visual and quantitative evidence that the dual-objective PSO framework achieves an effective balance between model simplicity and predictive power by implicitly optimizing the bias–variance trade-off. The percentage improvements in performance metrics and model complexity are summarized in **Fig. 11**. For the PSO-RF algorithm, the dominant parameters are the temperature, TaC, μ (mean), and Density, respectively. For the PSO-XGB algorithm, the dominant parameters are NBC, Temperature, μ (mean), Ni, HRC, TaC, Co, TiC, and Velocity, respectively.

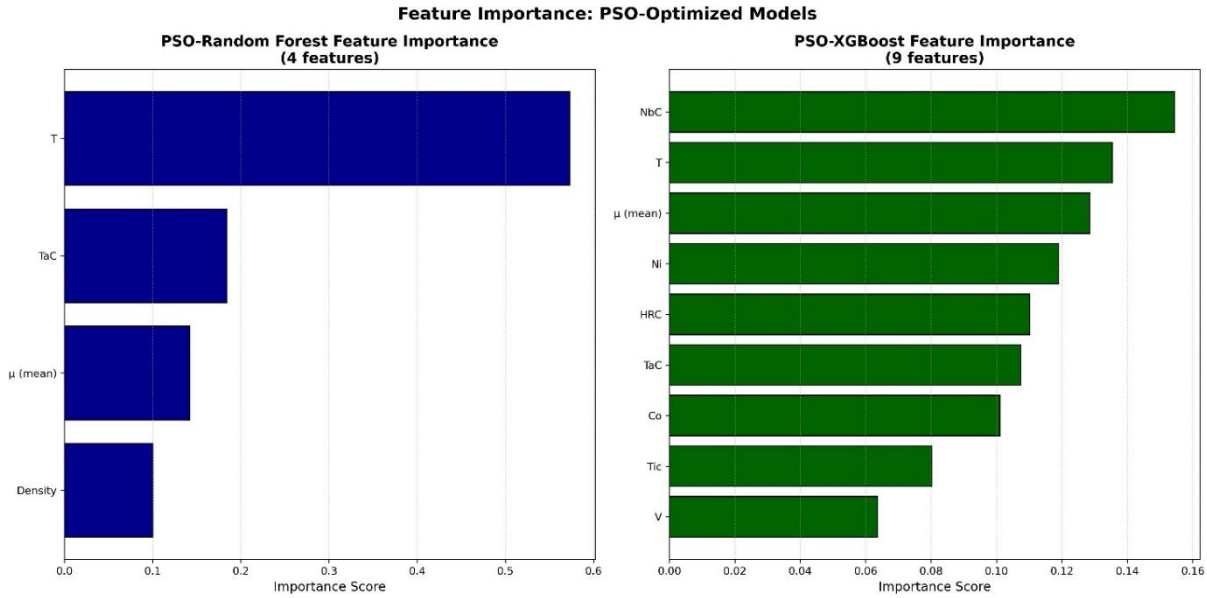


Fig.11 Summary of percentage improvements in performance metrics and model complexity.

6. Conclusion

This study investigated the effectiveness of a hybrid optimization framework combining Particle Swarm Optimization (PSO) with machine learning models for accurate wear rate prediction of WC/Co-based cermets. By simultaneously performing feature selection and hyperparameters tuning, the PSO algorithm adapted the Random Forest and XGBoost models to the dataset characteristics, improving predictive performance while controlling model complexity. Overall, the results demonstrate that PSO-based hybrid optimization is an effective strategy for improving machine learning models for wear rate prediction, enabling a balance between predictive accuracy, interpretability, and computational efficiency. Furthermore, future work should focus on expanding the dataset, applying advanced explainability techniques such as SHAP, and validating the models on independent datasets to further assess their robustness and generalization capability. The main conclusions are summarized as follows:

- The PSO algorithm successfully identified optimal hyperparameters configurations for both Random Forest and XGBoost, enhancing their predictive capability and performance.
- For the Random Forest model, PSO achieves a 67% reduction in dimensionality while maintaining reliable prediction accuracy.
- The PSO-optimized XGBoost model delivered the best overall performance, reaching an R^2 of 0.89 and reducing prediction errors by 20.57% (RMSE) and 21.26% (MAE) compared with the default model.

- While XGBoost provided the highest accuracy, the optimized Random Forest model offers a simpler and more interpretable solution.

Acknowledgments The authors are very grateful to our colleagues of Factory 05025 Algeria for their assistance in material elaboration, and sample preparation. A big Thanks to the team of laboratory of Metallic Materials Science ULg-MMS Belgium for testing and analysis of samples also electromechanical and Operational Safety Laboratory.

Author contribution Riad Harouz: Investigation, Formal analysis, Writing-original draft, Writing-review & editing. Khaled Khelil: Investigation, Formal analysis, Writing-original draft, Writing-review & editing. Djamel Zelmati: Investigation, Formal analysis, Writing-original draft, Writing-review & editing. Haithem Boumediri: Investigation, Formal analysis, Writing-original draft, Writing-review & editing.

Funding No funding.

Data availability The datasets generated and/or analyzed during the current study are included in the manuscript in the form of tables and figures. No additional data are available.

Declarations

Conflict of interest There is no conflict of interest.

References

1. Duman D, Gökçe H, Çimenoğlu H Synthesis, microstruc-ture, and mechanical properties of WC–TiC–Co ceramic compos -ites. J Eur Ceram Soc 32(7):1427–1433. https:// doi.org/ 10. 1016/j. jeurc erams oc. 2011. 06. 013 (2012).

2. Li Y, Liu N, Zhang X, Rong C Efect of WC content on the microstructure and mechanical properties of (Ti, W)(C, N)–Co cermets. Int J Refract Metal Hard Mater 26(1):33–40. https:// doi. org/ 10. 1016/j. ijrmhm. 2007. 01. 003 (2008).

3. Harouz, R., Boudebane, S., Lakehal, A., Derdy, O., Montrieux, H. M., Investigation of the tribological behaviour of WC/TiC based cermets in contact with Al2O3 alumina under high temperature, Journal of the Mechanical Behavior of Materials, 27(1-2) (2018). https://doi.org/10.1515/jmbm-2018-0004.

4. Bolognini S, Feusier G, Mari D, Viatte T, Benoit W.Int. J. Refract. Met. Hard Mater. 21, 19–29 (2003).

5. Chavanes A, Pauty E, Woydt M.Wear 256, 647–656 (2004).

6. Ostberg G, Buss K, Christenesen M, Norgren S, Andren HO, Mari D, Wahnström G, Reineck I.Int. J. Refract. Met. Hard Mater. 24, 135–144 (2006).

7. Yang QQ, Xiong WH, Li SQ, Dai HX, Li J.J. Alloys Compd. 506, 461–467(2010).

8. Yang QQ, Xiong WH, Li SQ, Yao ZH, Chen X.Corros. Sci., 52, 3205–3211(2010).

9. Li M-X, Wei W, Zhao Y, Li M, Huang H, Chen Z, Xie X-M, Liu X-B Fabrication and characterization of ceramic WC10Co4Cr-YSZ composite coating via HVOF spraying core-shell powders. Ceram Int (2025). https://doi.org/10.1016/j.ceramint.2025.02.085

10. LIANG, Xiaoliang, LIU, Zhanqiang, et WANG, Bing. Multi-pattern failure modes and wear mechanisms of WC-Co tools in dry turning Ti–6Al–4V. Ceramics International, vol. 46, no 15, p. 24512-24525(2020). https://doi.org/10.1016/j.ceramint.2020.06.238

11. Qiao Z, Yang R, Liu Y, Feng X, Huang J, Tian Y, Zhou P et al A feasible strategy to construct WC Co-Cr/cu composite coating with good tribo-corrosion behavior and anti-fouling properties for marine applications. Wear 564:205738 (2025). https://doi.org/10.1016/j.wear.2025.205738

12. Aristizabal, M., Ardila, L. C., Veiga, F., Arizmendi, M., Fernandez, J., Sánchez, J. M., Comparison of the friction and wear behaviour of WC–Ni–Co–Cr and WC–Co hardmetals in contact with steel at high temperatures, Wear, 280, pp. 15-21(2012).

13. Hussainova I (2003) Efect of microstructure on the erosive wear of titanium carbide-based cermets. Wear 255(1–6):121–128. https:// doi. org/ 10. 1016/ S0043- 1648(03) 00198-4

14. Park S, Jung J, Kang S, Jeong BW, Lee CK, Ihm J The carbon nonstoichiometry and the lattice parameter of (Ti1− xWx) C1− y. J Eur Ceram Soc 30(6):1519–1526. (2010). https:// doi. org/ 10. 1016/j. jeurc erams oc. 2009. 10. 022

15. Kwon H, Suh CY, Kim W Microstructure and mechanical properties of (Ti, W) C-Ni cermet prepared using a nano-sized TiC–WC powder mixture. J Alloy Compd 639:21–26(2015). https:// doi. org/ 10. 1016/j. jallc om. 2015. 03. 115

16. Choi JH, Gyawali G, Dhakal DR, Joshi B, Lee SW Elec -trodeposited Ni–W–TiC composite coatings: efect of tic rein -forcement on microstructural and tribological properties. Acta Metallurgica Sinica (English Letters) 33:573–582 (2020).

17. Li Y, Liu N, Zhang X, Rong C (2008) Efect of Mo addition on the microstructure and mechanical properties of ultra-fne grade TiC–TiN–WC–Mo2C–Co cermets. Int J Refract Metal Hard Mater 26(3):190–196. https:// doi. org/ 10. 1016/j. ijrmhm. 05. 005(2007).

18. Lee BG, Cho SW, Lee SW, Choi GS, Lim JW (2011) Oxygen efects on the mechanical properties and lattice strain of Ti and Ti-6Al-4V. Met Mater Int 17:733–736 (2011).

19. PEREIRA, P., VILHENA, L. M., SACRAMENTO, J., et al. Tribological behaviour of different formulations of WC composites. Wear, vol. 506, p. 204415 (2022). https://doi.org/10.1016/j.wear.2022.204415

20. TORKASHVAND, Kaveh, JOSHI, Shrikant, et GUPTA, Mohit. Advances in thermally sprayed WC-based wear-resistant coatings: Co-free binders, processing routes and

tribological behavior. Journal of Thermal Spray Technology, vol. 31, no 3, p. 342-377 (2022). https://doi.org/10.1007/s11666-022-01358-4

21. QIAO, Yunfei, LIU, YouRong, et FISCHER, Traugott E. Sliding and abrasive wear resistance of thermal-sprayed WC-Co coatings. Journal of Thermal Spray Technology, vol. 10, no 1, p. 118-125(2001). https://doi.org/10.1361/105996301770349583

22. USMANI, Saifi, SAMPATH, Sanjay, HOUCK, David L., et al. Effect of carbide grain size on the sliding and abrasive wear behavior of thermally sprayed WC-Co coatings. Tribology transactions, vol. 40, no 3, p. 470-478 (1997). https://doi.org/10.1080/10402009708983682

23. SONG, Bo, MURRAY, James W., WELLMAN, Richard G., et al. Dry sliding wear behaviour of HVOF thermal sprayed WC-Co-Cr and WC-CrxCy-Ni coatings. Wear, vol. 442, p. 203114 (2020). https://doi.org/10.1016/j.wear.2019.203114

24. JI, De-Hui, ZHUANG, Hui, HU, Qiang, et al. Effect of abrasive particle size on the tribological behavior of thermal sprayed WC-Cr3C2-Ni coatings. Journal of Alloys and Compounds, vol. 924, p. 166536 (2022). https://doi.org/10.1016/j.jallcom.2022.166536

25. WANG, Qihua, WANG, Xiaoyue, ZHANG, Xinrui, et al. Tribological properties study and prediction of PTFE composites based on experiments and machine learning. Tribology International, vol. 188, p. 108815(2023). https://doi.org/10.1016/j.triboint.2023.108815

26. CHEN, Shengshan, CHENG, Ganlin, GUO, Fei, et al. Integrating friction noise for in situ monitoring of polymer wear performance: a machine learning approach in tribology. Journal of Tribology, vol. 147, no 6, p. 061701(2025). https://doi.org/10.1115/1.4066947

27. MEZLINI, S., TKAYA, M. Ben, MANSORI, M. El, et al. Correlation between tribological parameters and wear mechanisms of homogeneous and heterogeneous material. Tribology Letters, vol. 33, no 2, p. 153-159 (2009). https://doi.org/10.1007/s11249-008-9403-5

28. KUKSENKO, V. S. et MAKHMUDOV, Kh F. Fracture in heterogeneous materials: experimental and theoretical studies. Russian Geology and Geophysics, vol. 58, no 6, p. 738-743 (2017). https://doi.org/10.1016/j.rgg.2016.09.030

29. WILLS, Jaime, CARO, Silvia, et BRAHAM, Andrew. Influence of material heterogeneity in the fracture of asphalt mixtures. International Journal of Pavement Engineering, vol. 20, no 7, p. 747-760 (2019). https://doi.org/10.1080/10298436.2017.1334461

30. VIEVERING, J., ONG, S., FOK, A., et al. Experimental Characterization of Spatial Randomness of Elastic Properties of Heterogeneous Materials. Experimental Mechanics, vol. 65, no 8, p. 1341-1355 (2025). https://doi.org/10.1007/s11340-025-01218-6

31. JI, Fengqin, LUO, Can, PANG, Ming, et al. Effect of WC particle size on the microstructural evolution and tribological properties of laser cladding Ti-bearing Co-based

WC reinforced coating. Surface and Coatings Technology, vol. 494, p. 131394 (2024).https://doi.org/10.1016/j.surfcoat.2024.131394

32. Srinath, G., and R. Gnanamoorthy. "Effect of short fibre reinforcement on the friction and wear behaviour of nylon 66." Applied Composite Materials 12.6 369-383(2005).

33. BOLELLI, Giovanni, BÖRNER, Tim, MILANTI, Andrea, et al. Tribological behavior of HVOF-and HVAF-sprayed composite coatings based on Fe-Alloy+ WC–12% Co. Surface and Coatings Technology, vol. 248, p. 104-112 (2014). https://doi.org/10.1016/j.surfcoat.2014.03.037

34. ZHU, Guanghui A., CHEE, K.-W.(GH) A., AHMED, Tauseef, et al. Tribological performance and corrosion resistance of HVOF WC-17 wt.% Co coatings: influence of micro-to-nanoscale morphology. The International Journal of Advanced Manufacturing Technology, vol. 128, no 9, p. 4091-4102 (2023). https://doi.org/10.1007/s00170-023-11943-8

35. BIRADA, Lakshmi Manasa, PULLELA, Vyshnavi, et THELLA, Babu Rao. Triboinformatic machine learning model for frictional behavior and wear volume loss prediction of SS316L alloy clad with WC/NiCrBSi. Journal of Bio-and Tribo-Corrosion, vol. 10, no 3, p. 68 (2024). https://doi.org/10.1007/s40735-024-00874-w

36. Talbi, N., Mehdi, O., Rashid, F.L. et al. Precision fault diagnosis in screw compressors using ANN. Int J Adv Manuf Technol (2026). https://doi.org/10.1007/s00170-026-17631-7

37. TANG, Xin, MAO, Ruipeng, ZHANG, Fan, et al. Optimizing WC-10Co cemented carbides with high-entropy (Ti, Cr, V, Nb, Mo)(C, N) inhibitor: Microstructure, mechanics, and wear resistance. Journal of Alloys and Compounds, vol. 1037, p. 182148 (2025). https://doi.org/10.1016/j.jallcom.2025.182148

38. JIANG, Dazhi, WANG, Guangjin, DONG, Wei, et al. Recent advance on metal carbides reinforced laser cladding coatings. Molecules, vol. 30, no 8, p. 1820 (2025). ; https://doi.org/10.3390/molecules30081820

39. HUANG, S. G., VLEUGELS, Jef, MOHRBACHER, Hardy, et al. Microstructure and tribological performance of NbC-Ni cermets modified by VC and Mo2C. International Journal of Refractory Metals and Hard Materials, vol. 66, p. 188-197(2017). https://doi.org/10.1016/j.ijrmhm.2017.03.012

40. AZEVÊDO, Heytor VSB, RAIMUNDO, Rafael A., MORAIS, Luís MF, et al. Microstructure, Mechanical and Tribological Properties of the x SiC—(1-x) WC—10 wt.% Co Composites Prepared by High-Energy Milling and Spark Plasma Sintering: Azevêdo, Raimundo, Morais, Junior, Barreto, Cavalcante, Filgueira, and Gomes. JOM, vol. 75, no 5, p. 1660-1671 (2023).https://doi.org/10.1007/s11837-023-05754-1

41. SHAH, Raj, JARAMILLO, Rudy, THOMAS, Garvin, et al. Artificial intelligence and machine learning in tribology: selected case studies and overall potential. Advanced Engineering Materials, vol. 27, no 23, p. 2401944(2025). https://doi.org/10.1002/adem.202401944

42. WATSON, Michael, CHRISTOFOROU, Peter, HERRERA, Paulo, et al. An analysis of the quality of experimental design and reliability of results in tribology research. Wear, vol. 426, p. 1712-1718(2019). https://doi.org/10.1016/j.wear.2018.12.028

43. CHERGUY, Oussama, CHMIELOWSKI, Radoslaw, HACHEM, Elie, et al. Deep Learning Prediction of Dry Friction in DLC Coatings Using Literature-Derived Data. Tribology Letters, vol. 73, no 4, p. 125(2025). https://doi.org/10.1007/s11249-025-02056-2

44. PATURI, Uma Maheshwera Reddy, PALAKURTHY, Sai Teja, et REDDY, N. S. The role of machine learning in tribology: A systematic review. Archives of Computational Methods in Engineering, vol. 30, no 2, p. 1345-1397 (2023).https://doi.org/10.1007/s11831-022-09841-5

45. Talbi, N., Boussaha, E.H., Terbah, R. et al. Machine learning algorithms for optimization of bearing fault diagnosis in wind systems: a comparative study. Int J Adv Manuf Technol 142, 2675–2691 (2026). https://doi.org/10.1007/s00170-025-17124-z

46. HASAN, Md Syam, KORDIJAZI, Amir, ROHATGI, Pradeep K., et al. Triboinformatic modeling of dry friction and wear of aluminum base alloys using machine learning algorithms. Tribology International, vol. 161, p. 107065 (2021). https://doi.org/10.1016/j.triboint.2021.107065

47. Qazani, M.R.C., Amini, S., Pedrammehr, S. et al. A machine learning method for cutting parameter selection in rotary ultrasonic-assisted end grinding. Int J Adv Manuf Technol 126, 1577–1591 (2023). https://doi.org/10.1007/s00170-023-11196-5

48. Bin Abu Sofian ADA, Lim HR, Siti Halimatul Munawaroh H, Ma Z, Chew KW, Show PL (2024) Machine learning and the renew able energy revolution: exploring solar and wind energy solutions for a sustainable future including innovations in energy storage. Sustain Dev 32:3953–3978

49. Han Z, Liu Y, Zhao J, Wang W Real time prediction for converter gas tank levels based on multi-output least square support vector regressor. Control Eng Pract 20(12):1400–1409. https:// doi. org/ 10. 1016/j. conen gprac. 08. 006. (2012).

50. NAJJAR, Ismail, SADOUN, Ayman, ALAM, M. N., et al. Prediction of wear rates of Al-TiO2 nanocomposites using artificial neural network modified with particle swarm optimization algorithm. Materials TodayCommunications,vol.35,p.105743(2023). https://doi.org/10.1016/j.mtcomm.2023.105743

51. Chen S, Cheng G, Guo F, Jia X, Wen X Integrating friction noise for in situ monitoring of polymer wear performance: a machine learning approach in tribology. J Tribol (2025). https://doi.org/10.1115/1.4066947

52. Golla CB, Narasimha Rao R, Ismail S Triboinformatics approach for prediction of high-stress abrasive wear and coefficient of friction in Al/TiC nanocomposites using machine learning techniques (2025). J Tribol. https://doi.org/10.1115/1.4066415

53. Wu D, Jennings C, Terpenny J, Gao RX, Kumara S A comparative study on machine learning algorithms for smart manufacturing: tool wear prediction using random forests. J Manuf Sci Eng 139(7):071018 (2017). https:// doi. org/ 10. 1115/1. 40363 50

54. Alagarsamy SV, Balasundaram R, Ravichandran M, Mohanavel V, Karthick A, Devi SS Taguchi approach and decision tree algorithm for prediction of wear rate in zinc oxide-flled AA7075 matrix composites. Surf Topogr Metrol Prop 9(3):035005 (2021). https:// doi.org/ 10. 1088/ 2051- 672X/ ac0f34

55. Tarca AL, Carey VJ, Chen X-W, Romero R, Dra S Educa -tion machine learning and its applications to biology. PLoS Com -put Biol 3(6) (2007).

56. HAROUZ, Riad, ZELMATI, Djamel, et KHELIL, Khaled. Machine learning application for wear rate prediction of WC/Co-based cermet with different content of Ni, Cr, TiC, TaC, and NbC. The International Journal of Advanced Manufacturing Technology, vol. 135, no 11, p. 5945-5959 (2024). https://doi.org/10.1007/s00170-024-14862-4

57. JATAVALLABHULA, Jagadesh Kumar, SHABANA, Shabana, et PAPPULA, Bridjesh. Development and evaluation of machine learning based predictive models for tribological properties of blended coatings at elevated temperature. Journal of Bio-and Tribo-Corrosion, vol. 11, no 1, p. 25 (2025). https://doi.org/10.1007/s40735-025-00952-7

58. GRZESIK, Wit, ATTIA, Helmi, WEGENER, Konrad, et al. Intelligent Methods for Quantifying and Determining Friction in the Cutting Process-a Review. Journal of Machine Engineering,(2026).
DOI: https://doi.org/10.36897/jme/218157

59. STOJANOVIĆ, Blaža, GAJEVIĆ, Sandra, KOSTIĆ, Nenad, et al. Optimization of parameters that affect wear of A356/Al2O3 nanocomposites using RSM, ANN, GA and PSO methods. Industrial Lubrication and Tribology, vol. 74, no 3, p. 350-359 (2022). https://doi.org/10.1108/ILT-07-2021-0262

60. Hasanipanah, M., Amnieh, H. B., Arab, H., & Zamzam, M. S. Feasibility of PSO-ANFIS model to estimate rock fragmentation produced by mine blasting. Neural Computing and Applications, 30, 1015–1024 (2018). https://doi.org/10.1007/s00521-016-2746-1.

[61] Aydın, M., Karakuzu, C., Uçar, M., Cengiz, A., & Çavuşlu, M. A. Prediction of surface roughness and cutting zone temperature in dry turning processes of AISI304 stainless steel using ANFIS with PSO learning. International Journal of Advanced Manufacturing Technology (2013). https://doi.org/10.1007/s00170-012-4540-2.

62. SARAT BABU, Mulpur. A Machine Learning (Gramian Angular Field+ SVR-PSO) Model for In-Process Cutting Tool Wear Assessment Using Multisensor Heterogeneous Data Fusion. Journal of Tribology, vol. 148, no 3, p. 034205(2026). https://doi.org/10.1115/1.4070059

63. Xu,L., Huang, C., Li, C., Wang, J., Liu, H., and Wang, X., "Estimation of Tool Wear and Optimization of Cutting Parameters Based on Novel ANFIS-PSO Method Toward Intelligent Machining," J. Intell. Manuf., 32(1), pp. 77–90(2020).

64. MODANLOO, Vahid, ELYASI, Majid, LEE, Taeyong, et al. Modeling of tensile strength and wear resistance in friction stir processed MMCs by metaheuristic optimization and supervised learning. The International Journal of Advanced Manufacturing Technology, 2025, vol. 139, no 5, p. 3095-3118. https://doi.org/10.1007/s00170-025-16070-0

65. GHORBANI, Ebrahim et YAGIZ, Saffet. Predicting disc cutter wear using two optimized machine learning techniques. Archives of Civil and Mechanical Engineering, vol. 24, no 2, p. 106 (2024). https://doi.org/10.1007/s43452-024-00911-y

66. B. Sun, H.M. Liu, J.Y. Tang, S.F. Rong, J. Manuf. Process. 117, 40–58 (2024). https://doi.org/10.1016/j.jmapro.2024.02.025

67. XIA, Tao, CHEN, Yixin, SONG, Tianpeng, et al. Optimization of Heat Treatment Process Parameters for 8Cr4Mo4V Bearing Ring Using FEA-NN-PSO Method. Metals and Materials International, vol. 31, no 9, p. 2776-2796. https://doi.org/10.1007/s12540-025-01909-8(2025).

68. CHEN, Bowen, LI, Ke, HOU, Yao, et al. Machine learning-based prediction of wear for GH4169 alloy at different temperatures, loads, and displacements. Materials Today Communications, vol. 46, p. 112878(2025).https://doi.org/10.1016/j.mtcomm.2025.112878

69. Parsopoulos, K.E., Vrahatis, M.N.. Particle swarm optimization and intelligence: Advances and applications. Information Science Reference, New York (2010).

70. Khelil, J., Khelil, K., Ramdani, M., & Boutassita, N.. Discrete wavelet design for bearing fault diagnosis using particle swarm optimization. Journal Européen des Systèmes Automatisés, 53(5) (2020). https://doi.org/10.18280/jesa.530513

71. Shi, Jinrong, et al. "Advances in the Application of Machine Learning in Composite Materials." Applied Composite Materials 33.1 : 42 (2026).